Prediction of ASTM Method D86 Distillation of Gasolines and Naphthas according to the Fugacity-Filmmodel from Gas Chromatographic Detailed Hydocarbon Analysis

Walter Spieksma
AC Analytical Controls, Rotterdam, the Netherlands

Abstract

Light refinery streams and finished gasolines are analyzed with different gas chromatography methods. Kováts indices and mole fractions of the components are used to determine physico-chemical properties. These properties are used in the fugacity-filmmodel, obtained from the combination of Fick's Law and Henry's Law. Calculated temperature/volume data are compared with experimental data from the 1996 80-laboratory crosscheck of ASTM D86 distillation within the standard deviation.

Introduction

In the petrochemical industry, light hydrocarbon mixtures such as gasolines and naphthas are produced from crude oil using the refinery process. Since 1927, the boiling range has been measured by rate-controlled distillation of a 100-mL sample according to the American Society of Testing and Materials (ASTM) method D86. Operation of the distillation towers is based on volatility and compositional data obtained from this D86 distillation. Also, gasoline specifications include the D86 boiling range. Gas chromatography (GC) offers much more compositional detail than D86 distillation and requires less operator time per sample. GC should replace D86 distillation; however, the pure component boiling points of separated GC peaks differ in nature from D86 boiling points (1). Despite the effort of many early researchers to link GC data to distillation performance (2), this discrepancy has not yet been solved.

Mixture boiling points depend on pure liquid vapor pressures, mole fractions, and activity coefficients of all components (3), whereas GC retention depends on vapor pressure and activity coefficient in the stationary phase only (4). In D86 distillation, component molecules are surrounded by the other molecules in the mixture. In symmetrical GC zones, only stationary phase polymer surrounds the analyte molecules.

A correlation between D86 distillation and GC analysis according to ASTM D2887 was developed to obtain the D86 boiling curve from simulated distillation (SimDis) (5). SimDis analysis (ASTM method D2887) involves signal integration and baseline subtraction. It is assumed that weight fraction is equal to area fraction (6). The retention time scale is calibrated with the boiling points of the *n*-paraffins. The SimDis initial and final boiling points (IBP and FBP) are located at the first and last 0.5% weight of the chromatogram, respectively. Butler (6) noted that SimDis IBP is lower than the D86 distillation temperature at the first recovered drop (IBP). The SimDis FBP is higher than the maximum D86 temperature achieved (FBP) (6). The correlation was modified for use with ASTM GC method D3710, which identifies volatiles in gasolines, etc. Precision of D86 distillation temperatures calculated with the modified correlation shows variation with the season of the year and the blending of the gasoline (7).

Detailed hydrocarbon analysis (DHA) of gasolines and naphthas with capillary GC according to ASTM method D5134 cannot be used in the D2887 correlation (5). D5134 also employs dimethylsilicone stationary phases, and *n*-paraffins are used to calculate Kováts indices of all peaks. The constant response factor assumption in SimDis is avoided in DHA by using theoretical response factors. The Kováts index is not only useful for compound identification, but can also be used to calculate vapor–liquid equilibrium data (4). A non-equilibrium transport model is required for model D86 distillation. To meet this demand, de Bruine and Ellison (8) used a one-tray distillation model. Obviously, the droplet at the D86 thermometer tip is not a tray; therefore, the temperatures calculated by the tray model have to be correlated with D86 temperatures.

In this paper, ASTM method D86 distillation is calculated from DHA data with the fugacity-filmmodel of mass transport. The calculated results are compared with experimental D86 distillation data.

Experimental

Samples were analyzed without dilution. Small injection volumes (0.1 L) and a split ratio of 200:1 were employed. DHA reported Kováts indices and weight fraction. Peaks were identified using the Kováts index. The theoretical flame ionization detector (FID) response factor, given in ASTM method D5443, was calculated from the carbon/hydrogen ratio in the molecule. Weight fractions were calculated from the areas of all peaks and the theoretical response factors. Density and molar mass were used to calculate volume and mole fractions, respectively (9). Chromatograms were represented in percent volume and Kováts index bar graphs (Figures 1–3).

An isomerate sample was analyzed according to a DHA method obtained from Analytical Controls (9) (Figure 1, Table I). SimDis analysis was also performed on this sample, and the D86 result of the correlation (5) is given in Figure 4 along with results of the Fugacity-Filmmodel. A Raffinate sample (Figure 2) was also analyzed according to DHA (Table I). The D86 result is given in Figure 5. Five ASTM D86 crosscheck gasolines from 1996 were analyzed by DHA X using a short 5%-phenyl precolumn to enhance the separation of aromatics from non-aromatics (Table I). The chromatogram of the March sample is given in Figure 3 and the D86 result is displayed in Figure 6. The samples are given in the legend of Figure 7.

The D86 distillation of five crosscheck samples was performed by approximately 80 laboratories in March, May, June, July, and September of 1996. The ASTM method D86 distillation of the other samples were performed only once. The D86 method is presented here in short, because these experimental conditions have to be modeled. The ASTM method D86 distillation prescribes thermometer readings to be recorded along with recovered liquid volume. An aliquot of 100 mL was put into a boiling flask and recovered from the condenser using a 100-mL graduated cylinder. Vapor from the boiling sample in the flask rose to the thermometer and a droplet was formed (Figure 8). A part of the most volatile components encountered in naphthas and gasolines did not condense in the icewater-cooled condenser. This was reported as loss. At the IBP, the first droplet appeared at the outlet of the cooling section. From IBP, the rate of distillation was adjusted to 4.5 mL/min recovered liquid until 5 mL residue was left in the flask. The FBP was the maximum temperature recorded. At FBP, all liquid sample had evaporated from the boiling flask that contained heavy vapor residue. After cooldown, the residue condensed to liquid

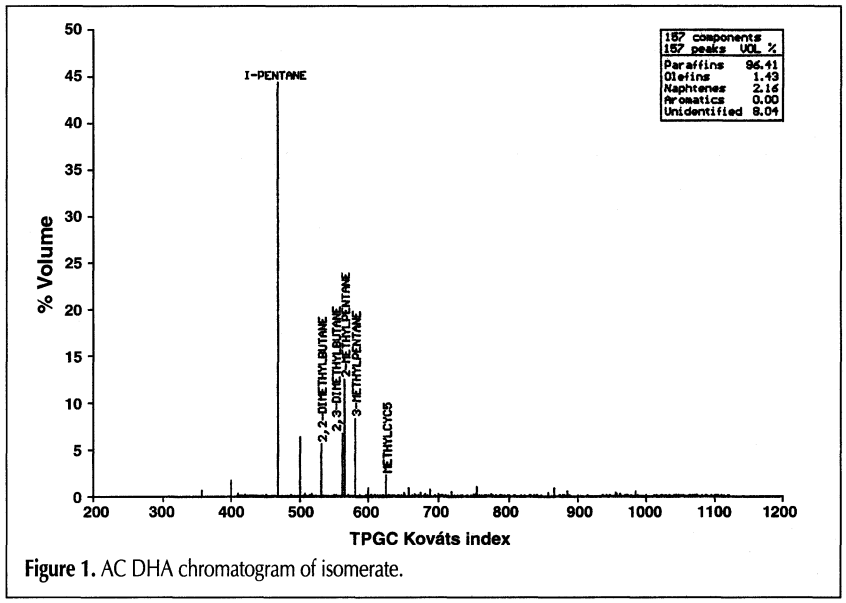

Figure 1. AC DHA chromatogram of isomerate.

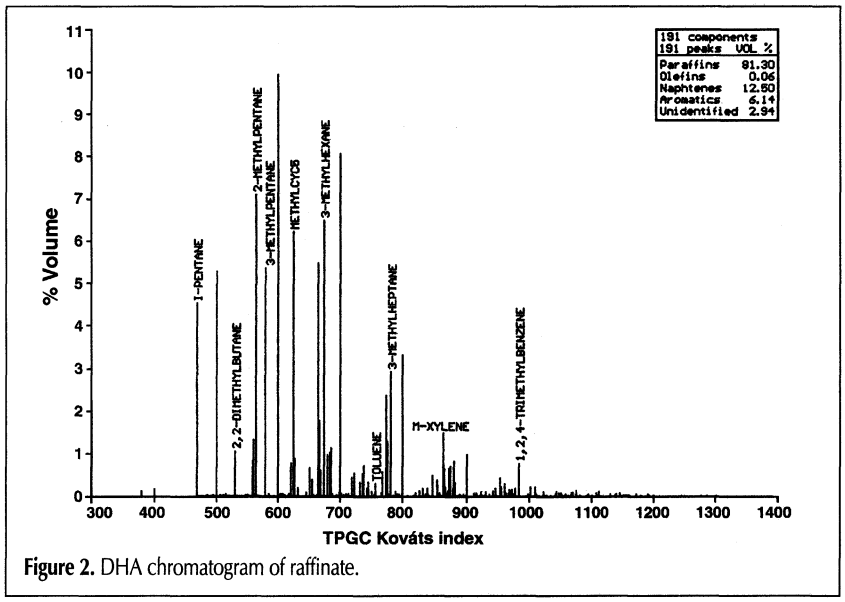

Figure 2. DHA chromatogram of raffinate.

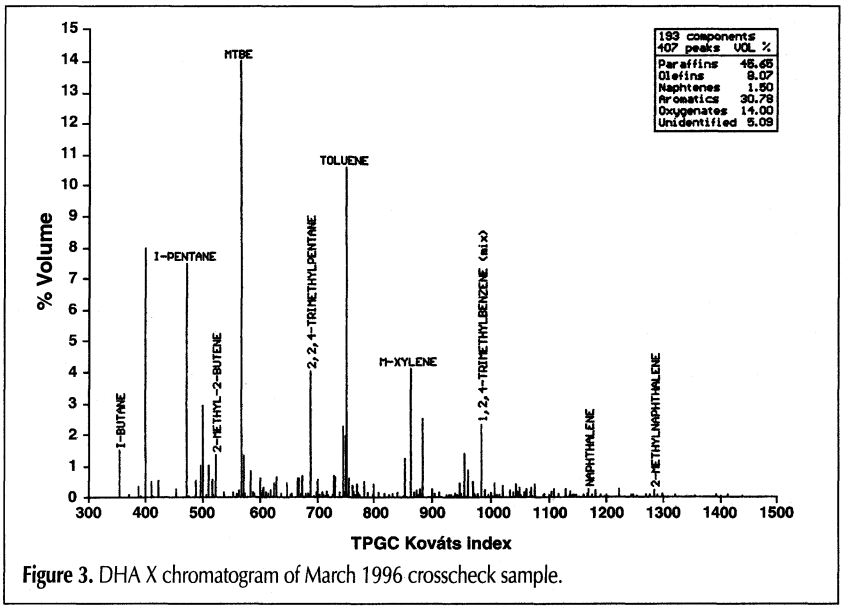

Figure 3. DHA X chromatogram of March 1996 crosscheck sample.

in the boiling flask. Because of loss and residue, some of the 100-mL sample was not recovered. The volume of loss was calculated by subtracting the volume of residue from the unrecovered volume. ASTM D86 distillation temperature curves may be reported in evaporated volume, which is the sum of recovered volume and loss.

Theory

Equilibrium

Fugacity is the tendency of a component to escape from its phase compartment. The dimension of fugacity is force per area or Pascal (N/m^2). At equilibrium between liquid and vapor in a closed system, fugacities of all components in the liquid and gas phase are equal. Using Dalton's Law, the fugacity of component (i) in the vapor phase (G) is defined as

$$f_i^G = y_i P \qquad \text{Eq 1}$$

Gas phase fugacity corresponds to partial pressure, which is the product of component i mole fraction (y_i) and total pressure (P).

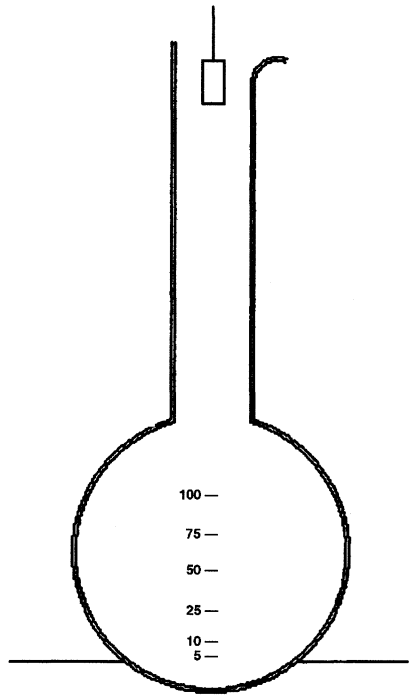

Figure 4. D86 distillation curve predicted from AC DHA of isomerate.

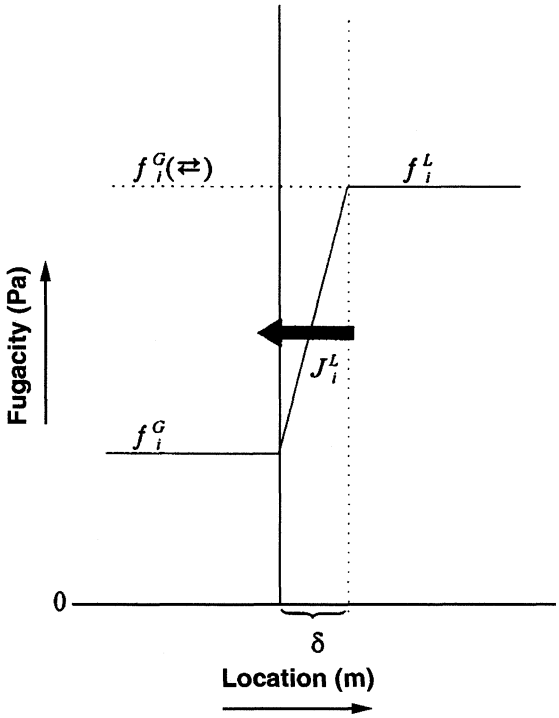

Figure 5. D86 distillation curve predicted from DHA of raffinate.

Table I. DHA Temperature Programmed Conditions

	DHA X (4)	AC DHA (4)	DHA*
Stationary phase	Dimethyl-silicone	Dimethyl-silicone	Dimethyl-silicone
Length [m]	100	50	50
Inner diameter [µm]	250	200	200
df [µm]	0.5	0.5	0.5
Precolumn	5 m DB-5	–	–
Mobile phase	He	He	He
t0 [min]	7.32	3.73	3.55
T1 [°C]	5	35	35
t1 [min]	10	30	30
r1 [°C/min]	5	2	2
T2 [°C]	50	200	70
t2 [min]	50	–	0
r2 [°C/min]	1.5	–	3
T3 [°C]	200	–	200
t3 [min]	5	–	–

* Results of GC analysis of the raffinate sample were provided by Dennis Sutton, Marathon Oil Company, TX.

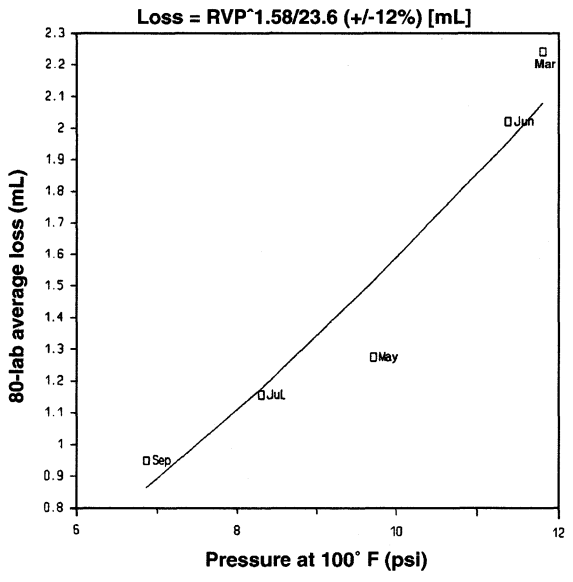

Figure 6. D86 distillation curve predicted from DHA X of March 1996 gasoline and the 80 laboratory crosscheck results.

The fugacity of component i in the liquid phase (L) is defined as

$$f_i^L = \gamma_i^L x_i P^i \qquad \text{Eq 2}$$

where x_i is the liquid mole fraction (obtained from DHA) and P^i is the pure liquid vapor pressure calculated from the Kováts retention index (also obtained from DHA).

Henry's law is found at equilibrium between vapor and liquid phase, when Eq 1 equals Eq 2:

$$y_i P = \gamma_i^L x_i P^i \qquad \text{Eq 3}$$

Luskin and Morris calculated the Reid vapor pressure (RVP) (ASTM method D323) of binary and ternary mixtures by summing Eq 3 at 100°F for all components. They estimated activity coefficients from aromatic molefraction (3). In this work, the activity coefficient (γ_i^L) was calculated according to the Wilson equation (10) for mixtures of N components:

$$\ln\gamma_i^L = 1 - \ln\left[\sum_i^N x_j \Lambda_{ij}\right] - \sum_k^N \frac{x_k \Lambda_{ki}}{\sum_j^N x_j \Lambda_{kj}} \qquad \text{Eq 4}$$

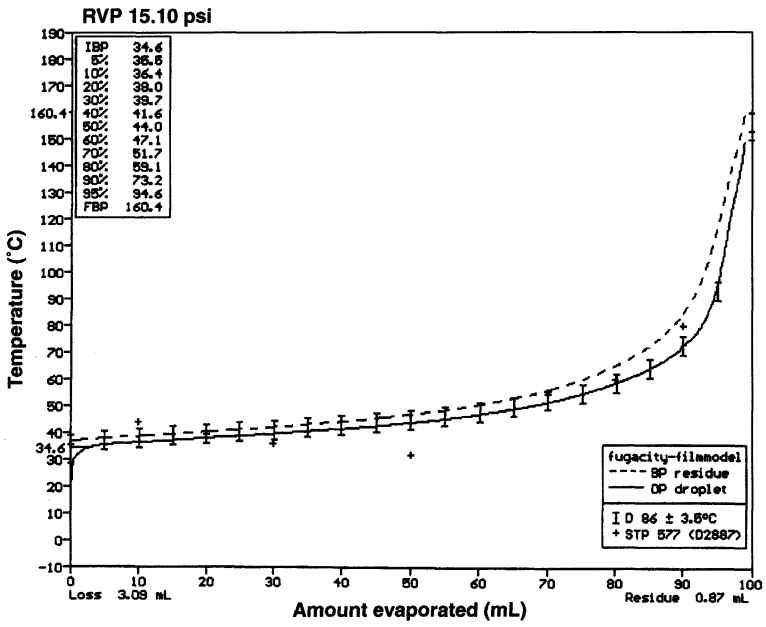

Figure 7. Difference between DHA X fugacity-filmmodel prediction and the mean of five 1996 ASTM D86 gasoline crosschecks of approximately 80 laboratories.

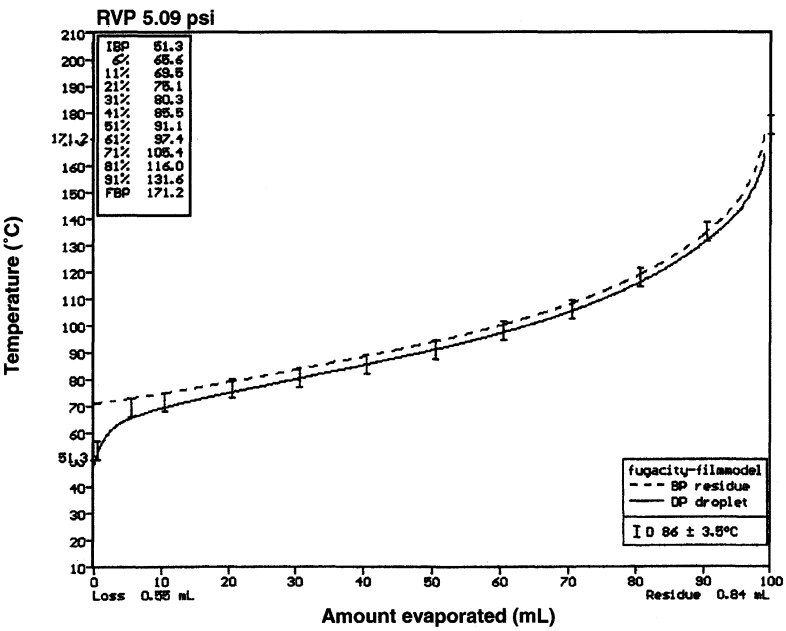

Figure 8. Geometry of ASTM D86 boiling flask, support, and thermometer tip.

The $N \times N$ matrix of Wilson binary parameters (Λ) is calculated from Kováts indices (4). Despite the fact that Eq 4 is the least complicated of available mixing equations (11), computation time rises steeply with the number of components. If Eq 4 is written out for a mixture of 100 components, 100 denominators appear with 100 terms. Even the current 200-MHz-processor computers are challenged by Eq 4.

Transport

ASTM method D86 distillation is performed in an open system. In the boiling flask, the heated liquid sample boils off. At the thermometer tip, components are exchanged between the vapor and the droplet by condensation and evaporation. Vapor returns to the liquid state in the condenser and is recovered in the graduate cylinder. This non-equilibrium system can attain steady state when the rates of evaporation and recovery are equal.

The fugacity-filmmodel of interphase mass transport combines fugacity (Eq 1 and 2) and diffusion and is based on three principles. First, Fick's Law states that the flux (J_i) of component i through a plane of thicknes ∂z is driven by concentration difference (∂C_i) and is limited by diffusion ($J_i = D_i \partial C_i / \partial z$ [mole/m^{2}s]). Second, according to Dalton's Law, gas phase concentration is related to vapor mole fraction y_i and total pressure by the formula $C_i^G = y_i P/RT$ [mole/m^3]. Third, Lewis defined gas phase fugacity (Eq 1) and liquid phase fugacity (Eq 2), which are equal at equilibrium.

It is assumed that diffusion D_i^L in a liquid interphase film with thickness δ[m] limits component transport. The resistance of the gas phase is ignored, because diffusion in gases is 1000 times faster than in liquids. Therefore, the evaporation flux (J_i^L) of component i through surface area A[m^2] can be written

$$J_i^L = \frac{-\partial n_i^L}{A\partial t} = \frac{D_i^L}{\delta RT}\left(f^L - f^G\right) \qquad \text{Eq 5}$$

which is shown in Figure 9. Both phases are supposed to be well-mixed; no gradients occur in the bulk of the phases. At equilibrium, gas phase fugacity f_i^G (⇔) equals liquid phase fugacity f_i^L, resulting in no flux. If fugacity f_i^G in the gas phase is higher than equilibrium fugacity f_i^G (⇔), condensation of component i into the liquid phase will occur according to the negative evaporation flux defined in Eq 5. The liquid film at the exchanging surface area is assumed to be a monomolecular layer of spherical molecules. The interphase liquid film thickness (δ) is calculated from the liquid molar volume (V^s) of the mixture and the Avogadro number N_A according to: $\delta = 1.204\sqrt{(V^s/N_A)}$[m]. Determination of exchanging surface area A may be feasible in case of a non-boiling liquid but is not feasible in the case of a turbulent rising stream of expanding vapor bubbles in a boiling flask (e.g., ASTM method D86 distillation). Calculation of liquid mixture molar volume is given in the liquid diffusion calculations.

Diffusion calculations

Diffusion coefficients of component i at infinite dilution in solvent s are calculated with a version of the binary Stokes-Einstein expression, modified by Hayduk and Minhas (10).

$$D_i^{\infty} = 1.55 \cdot 10^{-12} \frac{V^{s0.28}\, T^{1.29}\, \sigma^{s0.125}}{V^{i0.42}\, \eta^{s0.92}\, \sigma^{i0.105}} \qquad \text{Eq 6}$$

In the quasi-multicomponent approach (10), the solvent is taken to be a mixture. The mixture molar volume V^s is calculated from the mole fraction using

$$V^s = \sum_i^N x_i V^i \qquad \text{Eq 7}$$

Molar volumes V^i are calculated from molar masses and compound groups (4). Mole fractions of components in a distillation feed can determined from GC peak area (9). Multicomponent viscosity is calculated from the Grunberg and Nissan equation (10).

$$\ln\eta^s = \sum_i^N x_i \ln\eta^i + \sum_i^N \sum_{j\neq i}^N x_i x_j G_{ij} \qquad \text{Eq 8}$$

The cross-terms ($x_i x_j$) are ignored because most mole fractions are small and much calculation time is consumed if the cross terms are calculated for a 260 component system. The pure liquid viscosities η^i are estimated according to van Velzen, Cardozo, and Langenkamp (10) from molar mass and the functional group of the components i determined by GC (4). The multicomponent surface tension is calculated from the parachor (P_i) according to McLeod-Sugden (10).

$$\sqrt[4]{\sigma^s} = \sum_i^N [P_i]\left[\frac{x_i}{V^i} - \frac{y_i P}{RT}\right] \qquad \text{Eq 9}$$

At low pressure, the vapor mole fraction term is ignored. Surface tension depends more on liquid composition than on temperature (10). In the vapor mole fraction term, vapor fugacity (Eq 1) is recognized. In this paper, the vapor term was applied. The parachor (P_i) is calculated from molecular structure (10). In this paper, the parachor was estimated only from molar mass and compound group as determined by GC analysis (4).

Concentration effects on diffusion coefficients of components i at infinite dilution D are accounted for by a thermodynamic factor (12). The thermodynamic factor uses a chemical potential model of mass transport. In this work, we found that the correction

$$D_i^s = D_i^{\infty}\, \gamma_i \qquad \text{Eq 10}$$

gave satisfactory results. On intuitive grounds, it is clear that repulsion of a molecule by a solvent ($\gamma_i^L > 1$) enhances its diffusion and attraction by the solvent ($\gamma_i^L < 1$) slows diffusion down.

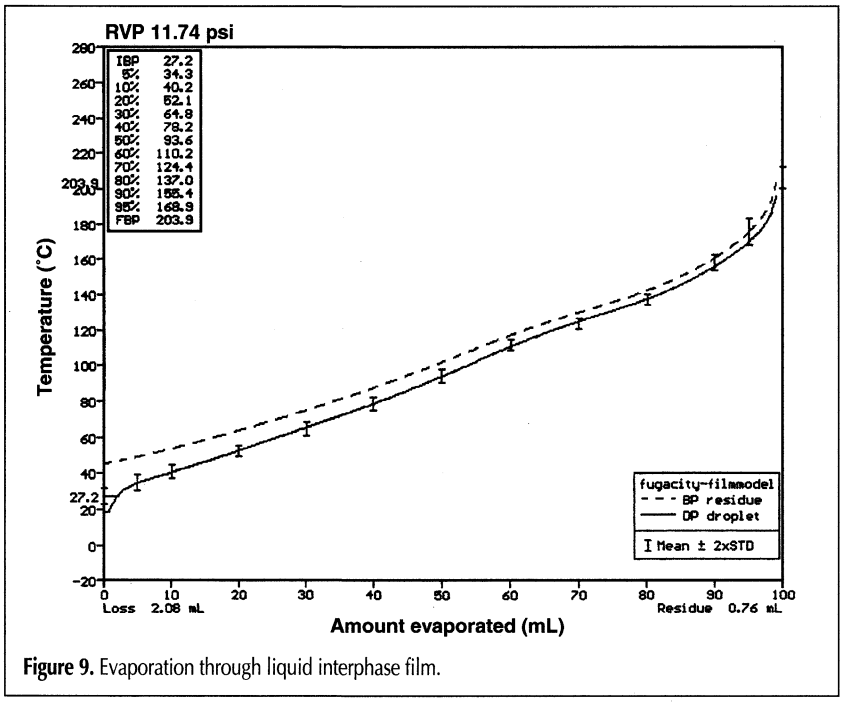

Figure 9. Evaporation through liquid interphase film.

Sample boil-off

The ASTM method D86 boiling flask was heated. When vapor bubbles appeared in the liquid sample, the sum of liquid fugacities (Eq 2) equaled barometric pressure (P). Isothermal liquid fugacities (Eq 2) are summed repeatedly until the temperature T_b is found, resulting in normal pressure (101325 Pa):

$$\sum_i^N \gamma_i^L x_i P^i(T_b) = 101325 \qquad \text{Eq 11}$$

If components are identified and mole fractions are determined by DHA, the normal boiling point (T_b) is fixed. T_b should not be confused with the boiling point reported in ASTM method D86 distillation. The value of T_b can only be measured with a thermometer immersed in the liquid sample in the boiling flask, which is certainly not prescribed in ASTM method D86.

After solving Eq 11, the three isothermal properties (vapor pressure, activity coefficient, and diffusion) in Equations 2 and 5 are fixed. The

only unknown property in the boiling phenomenon is the size of the liquid surface area A in Eq 5. In the flux ratio (J_i^L/J_r^L) of a component i and reference component r, this property is canceled because both components evaporate in the same boiling regime. Assuming that the rising of the vapor shifts vapor fugacity from equilibrium (Figure 9) for all components i equally ("ventilation"), integration of flux ratio in time Δt of Eq 5 results in

$$\frac{n_i^L(t+\Delta t)}{n_i^L(t)} = \left[\frac{n_r^L(t+\Delta t)}{n_r^L(t)}\right]^{\alpha_{ir}} \qquad \text{Eq 12}$$

with relative volatility α_{ir} defined as

$$\alpha_{ir} = \frac{D_i^L \gamma_i^L P^i}{D_r^L \gamma_r^L P^r} \qquad \text{Eq 13}$$

Eq 12 is only valid under isothermal and isocratic conditions, because relative volatility α_{ir} (Eq 13) is assumed to be constant in evaporation period Δt. Therefore, the evaporation process must be divided into small Δt steps. Period Δt is determined using Eq 12 in an indirect manner. Evaporated volume (V_{evap}) is the product of the number of moles evaporated and the molar volume V^i summed for all components i.

$$V_{evap} = \sum_i^N V^i(n_i^L(t) - n_i^L(t+\Delta t)) \qquad \text{Eq 14}$$

In steady state, the duration of evaporation period Δt can be found by dividing the evaporated volume (V_{evap}) by the recovery rate of 4.5 mL/min prescribed in ASTM D86.

The composition of the vapor that rises from the boiling off sample can be calculated with the mole fraction definition of the N components i.

$$y_i = \frac{n_i^G}{\sum_{i=1}^N n_i^G} = \frac{n_i^L(t) - n_i^L(t+\Delta t)}{\sum_{i=1}^N n_i^L(t) - n_i^L(t+\Delta t)} \qquad \text{Eq 15}$$

The amount of vapor (n_i^G) is the difference between the amounts of liquid before ($n_i^L[t]$) and after ($n_i^L[t+\Delta t]$) the evaporation period, Δt, obtained from solving Eq 12.

Droplet mass exchange

The vapor rising from the boiling sample reaches the thermometer tip and a droplet is formed. The maximum temperature of this droplet is the dewpoint (T_d), at which the sum of liquid fugacities (Eq 2) of N components i is equal to normal pressure.

$$\sum_{i=1}^N \gamma_i^d x_i P^i(T_d) = 101325 \qquad \text{Eq 16}$$

This equation is similar to Eq 11 except that liquid mole fraction x_i refers to the composition of the droplet. The condensation flux at T_d can be formulated according to Eq 5.

$$J_i^d = \frac{\partial n_i^d}{A\partial t} = \frac{D_i^d P}{\delta R T_d}\left(y_i - k_i^d x_i\right) \qquad \text{Eq 17}$$

Equilibrium constant (k_i^d) is defined by Henry's Law ($k_i^d = y_i/x_i = \gamma_i^d P^i/P$) (Eq 3). The vapor mole fraction y_i is obtained by solving Eq 15. Application of relative flux does not simplify Eq 17. Evaporation and condensation take place simultaneously, so gas phase fugacities f_i^G may rise or drop and the assumption of equal ratios f_i^G/f_i^G ($\Leftrightarrow$) in Eq 12 cannot be applied here. Consequently, exchanging surface area A of the droplet cannot be divided away like in Eq 12.

Integration of Eq 17 can be performed with the substitution of

$$\partial n_i^d = -\frac{n_t^d}{k_i^d}\,\partial\left(y_i - k_i^d x_i\right) \qquad \text{Eq 18}$$

The result of integrating Eq 17 over period Δt is

$$x_i(t+\Delta t) = \frac{y_i}{k_i^d} + \left[x_i(t) - \frac{y_i}{k_i^d}\right]\exp(-\Psi_i \Delta t) \qquad \text{Eq 19}$$

with flux freqency Ψ_i defined as

$$\Psi_i = \frac{A D_i^d \gamma_i^d P^i}{n_t^d\, \delta R T_d} \qquad \text{Eq 20}$$

Droplet mole fractions $x_i(t+\Delta t)$ after period Δt can be calculated with Eq 19. Calculation of the evaporation period (Δt) in Eq 20 is outlined in the section of this paper titled "Sample boil off". The flux frequency Ψ_i contains all physical properties involved in droplet mass exchange. If the flux frequency is very large ($\Psi_i \rightarrow \infty$), component i will achieve the liquid mole fraction in equilibrium with the vapor mole fraction after period Δt (Eq 3). If the flux frequency is very small ($\Psi_i \rightarrow 0$), the droplet mole fraction of component i does not change in period Δt according to Eq 19. Equilibrium achievement is enhanced by the large exchanging area A, fast liquid diffusion D_i^d, poor solubility or large activity coefficient γ_i^d, high vapor pressure P^i, a small total amount of droplet n_t^d, and a thin surface film. The mole fractions must be normalized to add up to 1 ($\Sigma x_i[t+\Delta t] = 1$). The assumptions behind Eq 19 and Eq 20 are that the amount of droplet n^d is constant and mole fractions x_i are small compared to 1.

The total number of moles of droplet n_t^d is estimated from the total volume of the droplet plus the liquid film suspended at the thermometer tip divided by liquid molar volume. In order to assess the exchanging surface area A, thermometer wetting should be considered.

Droplet suspended at thermometer tip. The diameter of a hanging droplet has a maximum diameter at which the droplet falls back into the boiling flask. This critical diameter depends on the the ratio of adhesion and gravity force, expressed in the Laplace number (La).

$$\text{Diameter}_{cr} = \sqrt[3]{\frac{6}{\pi}}\sqrt{\frac{La\sigma^d}{\rho^d g}} \qquad \text{Eq 21}$$

The value of La used is $6^{2/3}$ given by Smith et al. (13) and results in maximum drop diameters of about 4.5 mm. The density (ρ^d) is obtained from division of liquid molar volume (V^d) and molar mass (M^d) of the droplet. Molar mass is calculated using mole fractions (x_i) and molar masses (M^i) of the components in

the droplet ($M^d = \Sigma x_i M^i$).

Liquid layer on thermometer tip. The tip of thermometer 7 C prescribed by ASTM D86 has a length of 10–15 mm and a diameter of 5–8 mm. Assuming that liquid covers the entire thermometer tip, the contribution to surface area A is about 255 mm^2. Assuming that the liquid layer is approximately 0.3 mm thick, the volume contribution is 90 µL. A spherical droplet with a diameter of 4.5 mm contributes 48 µL to the suspended volume and 64 mm^2 to the exchanging surface area. The assumptions regarding liquid coverage of the thermometer tip are open to improvement. The droplet is small in comparison with the wet thermometer tip.

Initial and final conditions

The most important features of D86 are the IBP and FBP. The initial and final conditions are not steady state because the rate of evaporation does not equal rate of recovery.

At the moment that the first vapor hits the dry thermometer tip, the fugacity filmmodel cannot be applied, because a liquid phase must be present (Figure 9). It is assumed that at that moment, vapor condenses entirely on the thermometer tip, and the first vapor mole fractions (y_i) calculated with Eq 15 are used instead of liquid mole fractions (x_i) for the purpose of calculating the temperature T_d in Eq 20 (flux frequency).

Before IBP occurs in D86, some of the volatile components in gasolines and naphthas do not condensate in the condenser and are reported as loss. No fugacity-filmmodel of the ASTM method D86 condenser was developed. A correlation between RVP from DHA and loss (Figure 10) determined by the 80 laboratories in the ASTM D86 crosscheck gasolines is used.

If rate of evaporation is not known, evaporation period Δt is not known and Eq 19 cannot be applied before IBP. However, the rate of evaporation before IBP is given by the D86 prescription to reach IBP in 5–10 min. The heat required to warm up 100 mL of liquid sample from 18°C to the residue boiling point in 7.5 min is calculated with heat capacities and heat of non-ideal mixing. After bubbles appeared in the sample, it was assumed that the rate of 4.5 mL/min was reached within 5 mL evaporation. The D86 IBP is the dew point (Eq 16) calculated at the loss volume (Figures 7–9).

Before FBP of ASTM method D86 distillation, the recovery rate slows down. The power of the heating must be kept constant for the last 5 mL recovered. The thermometer tip is dry at FBP, and fumes appear in the boiling flask. The liquid in the boiling flask contains large vapor bubbles and foam that does not cover the entire heated bottom. A 3.829-mL amount of non-boiling liquid in tranquility will exactly cover the heated part of the bottom of the boiling flask. Geometrically, this corresponds to the diameter of the support (38 mm) of the 125-mL spherical flask. However, the foaming observed at FBP will leave part of the heated section not covered with liquid at larger residue volumes. The heat flux of the electrical heating enters the liquid over a smaller area. Then, the liquid evaporation rate slows down (and cracking fumes start to occur).

In the fugacity-filmmodel of D86, the power uptake of the sample from the heating is calculated with the evaporation rate at steady state. The value of the power uptake at 95 mL evaporation is maintained. Geometrically, the reduced power uptake of the last 3.829 mL of sample by partial heated bottom coverage is accounted for. Residue is calculated from the volume of remaining vapor in the boiling flask before the condenser. Assuming ideal gas behavior, the resulting liquid residue volume is quantitated. The D86 FBP is the boiling point (Eq 11) of the last residue (Figures 7–9).

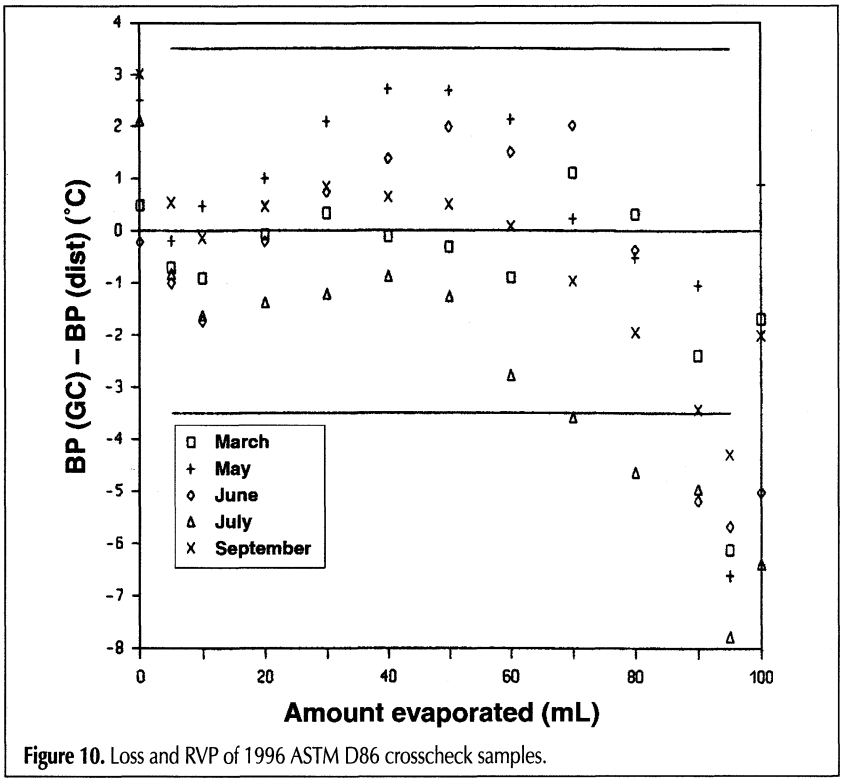

Figure 10. Loss and RVP of 1996 ASTM D86 crosscheck samples.

Results and Discussion

Calculations

ASTM method D86 distillation reports evaporated volumes and thermometer readings. Evaporated volume calculation is outlined in the "Sample boil off" section of this paper. The thermometer reads droplet dew points T_d determined by Eq 16. The calculation of loss is not based on the fugacity-filmmodel (Eq 5) but is taken from the RVP correlation line (Figure 10).

The mole fractions x_i from detailed hydrocarbon analysis, Kováts indices, and compound identification data are used. Vapor pressures P^i are calculated from Kováts index data (4). Activity coefficients γ^L are calculated from x_i and Kováts indices (4) with Eq 4. The RVP is calculated and is used to find loss (*Fig.*6). Then, diffusion coefficients are calculated as described.

At the beginning of D86 distillation, the terms in Eq 11 are determined from DHA. Using mole fractions x_i and molar volumes of components i (4), the quantities ($n^L[t]$ at $t = 0$) are calculated. In an iteration cycle, the boiling point T_b (Eq 5),

relative volatilities (Eq 13) at time t, and the new mole fractions (Eq 12) at time $t + \Delta t$ are calculated, resulting in a new boiling point (Eq 11), and so on.

The iterative cycle is driven by evaporation of a small amount ($n^{L \to G} \to 0$) of reference component r to satisfy the constant composition and temperature assumption (Eq 13) during evaporation period Δt. The evaporated amount ($n^{L \to G}$) is subtracted from the amount of reference component ($n^L[t]$) at time t to find the amount ($n_r^L[t + \Delta t]$) after the evaporation period ($n_r^L[t + \Delta t] = n_r^L[t] - n_r^{L \to G}$). Then, the amounts of all other components after evaporation are calculated using Eq 12 with relative volatility (Eq 13).

Next, mole fractions of all components in the rising vapor in period Δt are calculated with (Eq 15). The dewpoint T_d of the droplet is calculated with Eq 16. At dewpoint T_d, the equilibrium constant k_i^d and flux frequency (Eq 20) can be obtained using droplet diameter (Eq 21) and thermometer 7 C geometry. The new mole fraction is obtained from Eq 19 and results in a new dewpoint (Eq 16), an so on.

Peak lumping

Identification of all peaks is not always feasible with a single capillary column and an FID. Furthermore, Eq 4 computations in turbo-Pascal are limited to 259 components. Unidentified peaks are assumed to be alkanes with carbon number estimated from the temperature-programmed Kováts index.

$$n = \text{trunc}\left[\frac{I_i^s(T)}{100}\right] + 1 \qquad \text{Eq 22}$$

It follows that an unknown peak with an index (I_i^s) of 1078 is identified to be an iso-undecane. The number of peaks is reduced below 260 by lumping unknown peaks with mole fractions below 0.04 mole percent. The mole fractions (x_i and x_j) are summed and the Kováts index is averaged.

$$I_i^s(lump) = \frac{x_1 I_1^s + x_2 I_2^s}{x_1 + x_2} \qquad \text{Eq 23}$$

The properties of the unknown and lumped components are calculated according to the Kováts-Wilson model (4).

Results

The DHA chromatograms in Figures 1–3 have been converted to D86 distillation curves (Figures 7–9) with the fugacity-filmmodel. The isomerate sample was also analyzed according to ASTM D2887 for use in the STP 577 correlation (5). Whereas STP 577 predicts decreasing distillation temperatures from D2887, the fugacity-filmmodel predicts the measured curve within 3.5°C from AC DHA (Figure 4). The raffinate sample also displays agreement within 3.5°C (Figure 5). Both DHA and D86 were routinely performed on a refinery (results of GC analysis of the raffinate sample were provided by Dennis Sutton, Marathon Oil Company, TX). Five ASTM D86 monthly crosscheck gasolines are predicted from DHA X. The predicted March gasoline boiling curve entirely agrees within twice the standard deviation determined by approximately 80 laboratories in the USA (Figure 6). However, the dip at 95 mL evaporation of the May and July samples (Figure 7) falls outside the standard deviation limit. The May 1996 sample did not contain methyl-*tert*-butylether (MTBE); the four other samples contained more than 10% MTBE by volume.

Discussion

Major uncertainties in the fugacity-filmmodel of D86 distillation are the DHA peak identification in the heavy end of the chromatogram, thermometer wetting, loss in the cooling section that is not modeled, D86 FBP foam formation, and D86 FBP cracking of sample.

Nevertheless, the accuracy of D86 prediction from DHA is within several degrees Celsius. It is inevitable that peak identification of C10 and heavier compounds is prone to error. Application of GC–mass spectrometric analysis can be considered, but present-day routine instruments are not suited for fast GC operation. Thermometer wetting might be solved with the help of fluid dynamics, which is a quite involving area of research. The modeling of loss requires a vapor-diffusion-limited fugacity-filmmodel, which is not yet developed. The partial coverage of the boiling flask bottom at FBP (see Figure 8) can be solved with the evaluation of exchanging surface area in the boiling flask. If the depth of the remaining liquid is below 1 mm, foam formation will occur. Again, the solution to this problem may be found in fluid dynamics. Cracking of the heavy molecules might be evaluated with degradation reaction kinetics. If cracking products are not too light, they will condense in the condenser. The temperature of the cracking fumes may be equal to the boiling point of the remaining liquid foam. Therefore, it must be assumed that the fumes, after formation at the glass bottom wall, rise through the foam, which cools the cracking fumes.

Compared to the correlative model (5), one major advantage of the fugacity-filmmodel is that D86 parameters (e.g., heat-up time and recovery rate) can be adjusted. The model can be fine-tuned in a completely rational way, perhaps even using fluid dynamics. Another advantage is that the polarity of oxygen-containing ethers or alcohols (oxygenates) can be accounted for. A third advantage is that better identification of GC peaks will improve D86 predictions. A fourth advantage is that normal pressure is used. Whereas D86 results must be corrected if D86 is performed high above sea level, DHA analysis only requires a lower carrier gas pressure to maintain GC linear velocity.

Conclusion

D86 distillation of naphthas and gasolines can be predicted from DHA by virtue of the fugacity-filmmodel. The fugacity-filmmodel is based on Fick's Law and Henry's Law. The DHA fugacity-filmmodel of D86 distillation can predict experimentally determined boiling point ranges within several degrees Celsius.

Acknowledgments

The author would like to thank Dolf Grutterink (ASTM member at AC) for his effort to obtain test data from his world-

wide network and for sharing his knowledge of refinery streams. The author would also like to thank Bert Hoeks (AC) for checking mathematics and Hugo Knobel for critically reading the manuscript.

References

1. M.P.T. Bradley and C.E. Kennard. Volatility control by ASTM method D 2887-73, a feasibility study. pp 95–107.
2. *Calculation of Physical Properties of Petroleum Products from Gas Chromatographic Analysis*, J.B. Wheeler, H.M. Hoersch, C.E. Wilson, and E.J. McGlinchey, Eds. ASTM Special Technical Publication STP 577, American Society of Testing and Materials, 1975.
3. M.M. Luskin and W.E. Morris. Reid Vapor Pressure of Hydrocarbon Mixtures, pp 65–70.
4. W. Spieksma. Determination of vapor liquid equilibrium from the Kováts retention index on dimethylsilicone using the Wilson mixing model. *J. High Resol. Chromatogr.* (1997).
5. D.C. Ford, W.H. Miller, R.C. Thren, and R. Wertzler. Correlation of ASTM Method D2887-73 Boiling Range Distribution Data with ASTM Method D86-67 Distillation Data, pp 20–30.
6. Butler. Simulated distillation by gas chromatography. *Chromatographic Science Series, Vol. 11: Chromatography in Petroleum Analysis*, Altgelt and Gouw, Eds. (1979).
7. J.A. Crandall, R.K Bade, D.E. Clay, R.E. Warner, and S.B. Hunt. Simulated distillation application of gas chromatography: the real world. *Adv. Instrum. Control* : 605–637 (1990).
8. W. de Bruine and R.J. Ellison. *Calculation of ASTM Method D86-67 Distillation and Reid Vapor Pressure from the Gas–Liquid Chromatographic True Boiling Point*, p 9–19.
9. Operating manual for Detailed Hydrocarbon Analysis order no. 23060.004. AC Analytical Controls, Rotterdam, the Netherlands.
10. Reid, Prausnitz, and Poling. *The Properties of Gases and Liquids*, 4th ed. ISBN 0071002847, 1987.
11. Gmehling and Onken. Vapor–Liquid Equilibrium Data Collection DECHEMA chemistry series, 1977.
12. Ross, Taylor, and R. Krishna. *Multicomponent Mass Transfer*. Wiley & Sons, New York, NY, 1993.
13. Smith, Stammers, and Janssen. Fysische Transport Verschijnselen. DUM ISBN 9065620508, 1981.

Manuscript accepted July 14, 1998.